

UCLA

UCLA Previously Published Works

Title

Analytical insights into optimality and resonance in fish swimming

Permalink

<https://escholarship.org/uc/item/9dg3189z>

Journal

Journal of The Royal Society Interface, 11(92)

ISSN

1742-5689

Authors

Kohannim, Saba
Iwasaki, Tetsuya

Publication Date

2014-03-06

DOI

10.1098/rsif.2013.1073

Peer reviewed

Analytical Insights into Optimality and Resonance in Fish Swimming

Saba Kohannim and Tetsuya Iwasaki

Mechanical and Aerospace Engineering
University of California, Los Angeles
420 Westwood Plaza, Los Angeles, CA 90095
Email: {sabakohannim,tiwasaki}@ucla.edu

December 14, 2013

Abstract

This paper provides analytical insight into the hypothesis that fish exploit resonance to reduce the mechanical cost of swimming. A simple body-fluid fish model, representing carangiform locomotion, is developed. Steady swimming at various speeds is analyzed using optimal gait theory by minimizing bending moment over tail movements and stiffness, and the results are shown to match with data from observed swimming. Our analysis indicates the following: Thrust-drag balance leads to the Strouhal number being predetermined based on the drag coefficient and the ratio of wetted body area to cross-sectional area of accelerated fluid. Muscle tension is reduced when undulation frequency matches resonance frequency, which maximizes the ratio of tail-tip velocity to bending moment. Finally, hydrodynamic resonance determines tail-beat frequency, while muscle stiffness is actively adjusted so that overall body-fluid resonance is exploited.

Keywords: Fish Swimming, Optimal Locomotion, Resonance

1 Introduction

Fish swim by generating thrust through interactions between their body movement and the surrounding water. Studies of fish locomotion aim to understand how fish choose a frequency and pattern (gait) of tail oscillation, how thrust is generated efficiently through hydrodynamic forces, and how body shape and muscle activation are adjusted to regulate swim speed. Fish locomotion has been investigated using various methods, including kinematic and biomechanical data analysis of live fish, swimming experiments using flexible fish body models, and computational/experimental analyses of oscillating foils in fluids. Several theories have been formulated using these methods.

One prevalent theory is that fish minimize mechanical bending cost, or maximize thrust, by tuning their natural frequency to the tail-beat frequency [1, 2]. Studies suggest that fish use their muscles, skin, and tendons, to alter their body stiffness to achieve the required natural frequency [3, 4]. Previous studies on the relationship between tail-beat frequency, amplitude, and speed have concluded a linear relationship between speed and frequency [5, 6]. Experimental data on pumpkinseed sunfish suggest that fish increase their flexural stiffness to increase their tail-beat frequency to achieve faster swimming speeds, while maintaining constant tail-tip amplitudes [7].

Thrust production in swimming has been analyzed through vortex structure and energy expenditure of the wake. Experiments on foils oscillating in fluids have demonstrated that maximum thrust occurs when the nondimensional Strouhal number is within 0.25-0.35 [8], agreeing with values observed in biology 0.2-0.4 [9]. Optimum hydrodynamic efficiency is achieved when foil oscillation frequency coincides with the frequency of maximum spatial amplification of unstable wake [10], or “wake resonance frequency” [11, 12].

The goal of this paper is to provide simple analytical explanations for why fish choose a specific gait and oscillation frequency when swimming at a steady-state velocity. We first hypothesize that the natural gait is optimal and minimizes a mechanical cost. For instance, the natural gait may be minimizing muscle tension, power consumption, body shape curvature, or a combination thereof. Furthermore, we hypothesize that resonance is exploited in reducing the cost. Because both frequency tuning and hydrodynamic wake resonance have been observed, this resonance likely depends on both body and fluid dynamics. In contrast with previous works that focused on individual aspects of biomechanics and hydrodynamics of swimming, this paper presents an integrative view of fish swimming mechanisms, based on a simple model of body-fluid dynamics.

The primary analysis focuses on saithe (*pollachius virens*) swimming. Carangiform locomotion of saithe has been studied using Lighthill’s slender body theory by [13, 14, 15], which modeled saithe as a continuous dynamic beam under hydrodynamic forces and moments. Here, we develop a discrete model using three rigid bodies with two rotational joints that only permit lateral oscillation. We consider standard form drag on the whole body and added-mass effect on the tail for thrust generation [16, 17, 18] to model the resistive/reactive hydrodynamic forces. To determine whether natural swimming gait is optimal, we compare numerical results from model-based analysis to data from observed swimming. We find optimal gaits using the approach developed in [19], where tail motion is optimized to achieve a given average velocity with minimal mechanical cost. This simple method allows us to develop analytical insights into the connection between optimality and resonance, plus various properties including Strouhal number, power consumption, and Froude efficiency.

Our analyses suggest the following. The Strouhal number can be predetermined by the fish’s body geometry, and is independent of the gait and swim speed. The total power consumption in steady swimming is equal to twice the thrust power, regardless of the gait or oscillation frequency, and is only a function of velocity and fluid drag coefficient. Thus, the minimum-power optimal gait is not well defined. Minimizing the fish’s body curvature resulted in a trivial solution and will not be discussed. However, the optimal gait which minimizes bending moment or muscle tension, closely resembles observed swimming gait. Furthermore, minimizing muscle tension explains the observed tendency of increasing tail-beat frequency and stiffness to achieve higher velocities, while maintaining constant tail amplitude. The optimal frequency occurs at the resonance which maximizes the ratio of tail-tip velocity to bending moment; this resonance results from both the body resonance and the fluid resonance.

2 Materials and Methods

2.1 Body-Fluid Interaction Model

Saithe fish exhibit carangiform locomotion, where undulation is concentrated in the posterior half of the body. In our study, we use a simple model (see the Appendix for details) with three rigid bodies and two rotational joints (figure 1), representing a heavy head/trunk region (“main body”) and undulating precaudal and caudal regions (“tail”). The main body of the fish, with center of mass at (x_o, y_o) , is assumed to move only in the x -direction, with no rotation or translation in the y -direction, such that its motion is solely described by the position x_o and velocity $v := -\dot{x}_o$. This

assumption is reasonable for studying carangiform locomotion along a straight line. Tail motion is described by the angular displacements of the oscillating panels $\theta := (\theta_1, \theta_2)$ and is generated from the net effects of hydrodynamic forces and muscle bending moments.

The muscle bending moments consist of active and passive components [20]. The active component (u_1, u_2) results from the difference in antagonistic left/right muscle tensions and is directly controlled through motoneuron activation. The passive component results from co-contraction of left/right muscles plus intrinsic elasticity of the tissues, and is modeled proportional to the curvatures (angular displacements) at the two joints with proportionality constants (stiffnesses) k_1 and k_2 . Undulatory motion of fish is driven by anterior muscles in the precaudal region, and the resulting wave is propagated down the tail through the body’s passive stiffness [21, 22, 23]. To make our model similar to live fish, we allow the tail to oscillate passively; the active muscle bending moment u_1 is applied only at the anterior joint, with the posterior joint assumed passive, i.e. $u_2(t) \equiv 0$, unless otherwise noted.

[Figure 1 about here.]

In carangiform locomotion of saithe, with Reynolds number (Re) between 2×10^5 and 8×10^5 [13], thrust generation is dominated by reactive forces from water inertia [18]. Therefore, we only consider reactive thrust in the tail and resistive drag acting on the main body. The drag force f_o is proportional to the fish’s total (main body and tail) wetted surface area A_w and the square of the velocity v , with drag coefficient c_D , which is approximately 0.01 for swimming fish [18]. The mean thrust necessary to balance the drag is generated reactively in the undulating sections. In inviscid flow, this reactive force arises from the volume of water accelerated by the panels. The mass of the accelerated fluid adds to the fish’s body mass, for a total effective mass. We assume the volume of water accelerates in the lateral y -direction while sliding along the body in the tangential direction, so its x -position remains constant (figure 2). The reactive force f_i is normal to the panel, and its lateral component is proportional to the acceleration and mass of the water slice [24]. The fluid mass m_{A_i} is equal to the mass of the nominal cylindrical volume of water multiplied by the added-mass coefficient c_{A_i} , accounting for dependence of fluid flow on the tail shape. This reactive force model is equivalent to the spatial discretization of Lighthill’s slender-body theory [16, 25].

[Figure 2 about here.]

With the model for hydrodynamic forces and torques, nonlinear equations of motion (EOM) are derived from first principles of physics as in [26]. To gain insights into swimming mechanisms, we simplify the EOM assuming small oscillation angles. Additionally, we consider steady-state swimming at a constant average speed v resulting from periodic body movements θ , and take the average over a cycle to remove acceleration. Consequently, we get two simplified EOM. The first equation shows how the muscle bending moment u results in body motion θ , and the second equation shows the force balance between the total drag and the average thrust. A detailed derivation of the EOM is in the Appendix. Velocity fluctuations are ignored in the first EOM, adding limitations to the model. However, the simplification helps us find important properties in steady swimming otherwise hidden in a complicated mathematical model.

2.2 Model Parameters

We fix model parameters using data on the body dimensions, kinematics, and observed gaits of live saithe provided by [13, 14]. According to the data, a saithe, on average, travels approximately 86% of its body length in one tail-beat cycle. Therefore, a 40 cm saithe swims at approximately 1.2 m/s with a frequency of 3.5 Hz. The body dimensions of saithe and kinematic data, averaged over 13

video sequences, are given in table 1. Based on the distribution of amplitude of movement along the body, we approximate the main body to be 50% of the entire length, and approximate the undulating precaudal region and caudal tail fin to be 40% and 60% of the posterior half, respectively. The fish’s side view is given in figure 3, with body parameters in table 2.

[Figure 3 about here.]

[Table 1 about here.]

The saithe’s natural gait is described by the distribution of amplitude and phase of movement along the body length. Two observed gaits at two swim speeds are given in [13]. Snapshots of one observed gait, traveling at 1.2 m/s with an oscillating frequency of 3.49 Hz, are shown in figure 4, where the tail angles $\theta_{\text{nat}}(t)$ were determined by spatial discretization. For a 40 cm fish, the tail-tip amplitude y_{max} is approximately 3.3 cm. We define the nondimensional frequency called the Strouhal number, as $St = fh/v$, where f is the tail-beat frequency in Hertz, and $h = 2y_{\text{max}}$ is the peak-to-peak tail-tip amplitude. For an average fast-swimming saithe, the Strouhal number is about 0.20. This value is at the low end of the 0.2-0.4 range observed in fish and cetaceans [27].

[Figure 4 about here.]

The fluid drag depends on the drag coefficient c_D . According to [28], this value is approximately 0.01 for salmon and herring swimming at $Re \sim 10^6$. The averaged drag coefficient calculated from saithe data in [13] is $c_D \approx 0.009$, and we use this value for our analysis. The thrust generated in the undulating tail sections depends on added-mass coefficients c_{A_1} and c_{A_2} . The precaudal tail section is close to a rectangular panel and it is reasonable to approximate the added-mass coefficient $c_{A_1} \approx 1$; however, the caudal tail shape is not close to a rectangle, and calculating the exact value of c_{A_2} is tedious. To find a reasonable value for c_{A_2} , we compute the value that balances thrust and drag forces for the two observed gaits provided by [13]. Figure 5 plots the lines in the (c_{A_1}, c_{A_2}) plane on which the thrust and drag balance for the two observed gaits. Averaging c_{A_2} values at $c_{A_1} = 1$ gives $c_{A_2} = 2.53$. The fluid force parameters used in our analysis are summarized in table 2, where A_i is the cross-sectional area of the cylindrical fluid accelerated by the i th tail panel. Note that with this body division, A_1 and A_2 are approximately equal, leading to insightful results later.

2.3 Optimal Gait Analysis

Various periodic forcing of the bending moment results in different tail oscillation patterns (gaits), which may lead to different characteristics (e.g. efficiency) of swimming. To determine whether natural swimming gait is optimal, we compare the frequency and body oscillation shape observed in natural swimming with optimal gaits that minimize certain cost functions while maintaining a steady swimming speed.

Optimal gaits are specified as follows. We apply a sinusoidal bending moment at the anterior tail joint. The amplitude and frequency of the driving input are constrained so that the model fish swims at a prescribed average velocity in the steady-state, balancing thrust and drag. Among those satisfying this constraint, we choose the bending moment that gives the smallest value of a selected cost function. The optimal input, and hence the optimal gait at a prescribed velocity, are thus determined for a given set of body and fluid parameters. We have examined various cost functions including the power consumption and body curvature, and found that choosing the smallest amplitude of active bending moment gave the optimal gait closest to the observed motion; the result of this case will be reported below. The theory developed in [19] directly provides an analytical expression for the optimal gait (see Appendix for details). We will exploit the theory to gain insights into swimming mechanisms.

The same active bending moment can generate tail oscillations of different shapes depending upon the tail stiffness. Therefore, the stiffness value can have a large impact on the swimming performance. While observations and experiments in the literature provide preliminary results on how body flexibility varies with body position and speed, they do not provide actual values for live saithe body stiffness that can be used to determine k_1 and k_2 in our model. In fact, stiffness values are probably actively adjusted for a given speed through co-contraction of left/right muscles [2]. To test this hypothesis, we set k_1 to be a reasonable scalar multiple of k_2 , and include k_2 in the optimal gait problem as an adjustable parameter. We examine cases with various ratio k_1/k_2 , for a sensitivity study, since a definite relationship between the body flexibility at various points on the body is not known.

Overall, the frequency and amplitude of sinusoidal active bending moment u_1 and tail stiffness k_2 are optimized to achieve a given average speed with minimum amplitude of u_1 , while hydrodynamic and body geometry/mass parameters, and the stiffness distribution over the body, k_1/k_2 , are fixed. The optimization is repeated for various swim speeds in a range observed in saithe swimming to determine whether the observed gaits can be explained by optimality. When we examine hydrodynamic resonance in Section 3.2.3, the procedure is modified by assuming that the fish body has no mass or stiffness and both tail joints are driven by active muscle bending moments. In this case, tail stiffness parameters are set to zero ($k_1 = k_2 = 0$), and frequency, amplitudes, and phases of bending moments u_1 and u_2 are adjusted to minimize the sum of squares of the bending moment amplitudes.

3 Results

3.1 Intrinsic Properties of Steady Fish Swimming

Various tail oscillations of different frequency, shape, and amplitude lead to steady swimming at various speeds. There are certain properties that are shared by all swimming behaviors. This section presents such gait-independent intrinsic properties.

3.1.1 Strouhal Number

For the saithe model, with parameters given in Section 2.2, the virtual mass per unit length for panel 1 is roughly equal to that for panel 2, i.e. $A_1 \cong A_2 =: A_o$. In this case, the thrust-drag balance equation can be simplified to give the following expression for the ratio of the locomotion velocity v to the maximum lateral tail-tip velocity v_t :

$$\frac{v}{v_t} = \sqrt{\frac{A_o}{2c_D A_w}}. \quad (1)$$

Equation (1) implies that the average swimming velocity is proportional to the maximum tail-tip velocity, with a constant determined from only the fish's body geometry and hydrodynamic force parameters. If a fish has a large drag coefficient c_D or a large wetted area A_w , a higher tail-tip velocity v_t is required to achieve a given speed v . The relationship expressed in (1) agrees with observations from biology. Data on carangiform locomotion of live scombroid fish shows a linear relationship between swim speed and tail speed [29, 30]. This relationship was calculated by [31] to be $v/v_t = 1.21$ for steady swimming, and $v/v_t = 1.9$ for swimming starting from rest. Tail velocity also appears to be directly proportional to swim velocity in anguilliform swimming of eel [32]. In our model, we get $v/v_t = 1.57$, similar to the expressions found by [31], while live fish observation gives $v/v_t = 1.44$ [14].

The Strouhal number, $St = h/(v\tau)$, can be interpreted as the ratio of peak-to-peak tail amplitude h to the distance traveled over a cycle, $v\tau$. Because the maximum tail-tip velocity is $v_t = \pi h/\tau$ for sinusoidal oscillations, the Strouhal number can also be viewed as the ratio $St = (1/\pi)(v_t/v)$, leading to the expression:

$$St = \frac{1}{\pi} \sqrt{2c_D \cdot \frac{A_w}{A_o}}. \quad (2)$$

The relationship (1) between the locomotion velocity and tail-tip velocity makes St predetermined based on the fish's body geometry and fluid parameters, and independent of gait and velocity. Slow propulsion with fast tail-beat (higher St) results from a larger wetted area A_w , larger drag coefficient c_D , and/or smaller amount of water pushed by the tail A_o . The saithe model has $St = 0.2$, which is close to values observed for live saithe. If the virtual masses per unit length are not equal, i.e. $A_1 \neq A_2$, the expression for St in (2) remains with a new definition for A_o :

$$A_o := A_2 + (A_1 - A_2)(v_m/v_t)^2,$$

where v_m is the maximum lateral velocity of the posterior joint. Consequently, St may vary with the distribution of lateral velocity along the body.

3.1.2 Power Consumption and Froude Efficiency

In the literature, power consumption and Froude efficiency have been calculated using Lighthill's reactive theory for a continuum fish body model. In this study, we calculate these quantities using our discrete model. The calculated values will not be perfectly accurate due to the model simplifications, but provide new analytical insights into efficiency associated with swimming dynamics.

Basic power equations are obtained by multiplying the force EOM by velocity:

$$E = W + R + V, \quad \bar{D} = \bar{P}v, \quad (3)$$

where E is the power supplied by the muscle, W is the power lost into water, R is the rotational kinetic power, V is the elastic potential power, D is the power loss due to viscous fluid drag, and P is the thrust force. The bars indicate the average over a cycle. These quantities are defined in the Appendix. During steady swimming, the average kinetic and potential energies are constant. Thus, averaging the first equation in (3) yields $\bar{E} = \bar{W}$, indicating that the muscle power supply \bar{E} is equal to the power lost into water \bar{W} . Refer to Appendix for further detail. The second equation in (3) shows that the thrust power gained by the body through reactive hydrodynamic forces equals the power loss due to drag during steady swimming.

With the analytical formulas for W and P , one can verify through integral by parts that $\bar{W} = 2\bar{P}v$. This implies $\bar{E} = 2cv^3$, where $c := c_D\rho A_w/2$ is the fluid drag coefficient. Thus, the average total power consumption \bar{E} is estimated to be twice the power required for towing the fish body, and is independent of the body gait and oscillating frequency. Therefore, it does not make sense to optimize the gait to minimize power consumption because the total power \bar{E} is determined only by the velocity v and the fluid drag coefficient c , which are fixed in this analysis. The expression for \bar{E} arises from the work done to push fluid both axially and laterally, as explained in Section 4.1. For saithe, the power consumption at a nominal speed 1 m/s is estimated to be $\bar{E} = 0.58$ W. The average power consumption was calculated in [14] to be $0.0014\rho l_b^5 T^{-3}$ which equals 0.61 W for a 0.4 m fish swimming at 3.5 Hz. The Froude efficiency, or propulsive efficiency, is the ratio of useful power output to the total power consumption, $\eta := \bar{P}v/\bar{E}$. According to our result $\bar{E} = 2\bar{P}v$, the Froude efficiency is always equal to $\eta = 1/2$, regardless of the swimming gait, speed, hydrodynamic parameters, and body geometry.

3.2 Optimal Gait Analysis

3.2.1 Natural Gait is Optimal

This section examines whether the observed gait of saithe is optimal with respect to a certain cost function. The previous section revealed that total power consumption and Froude efficiency are independent of gait, and not appropriate cost functions for characterizing the natural gait in terms of an optimality. As an alternative, we minimize the muscle tension or bending moment cost. We solve for the optimal periodic body shape (amplitude and phase), oscillation frequency, and tail flexibility such that steady swimming at a desired average velocity is achieved. We compare the optimal gaits at various speeds with data on live saithe swimming provided by [13, 14] to examine optimality of the natural gaits. We also determine the role that body stiffness, driving frequency, and tail-tip amplitude play in varying the desired speed.

[Figure 5 about here.]

[Figure 6 about here.]

The results of the optimal gait calculations (figure 6) show that the optimal frequency ω_o increases linearly with locomotion velocity v . The optimal stiffness, k_{2_o} , exhibits polynomial growth with an increase in velocity. It can be analytically verified that optimal ω_o and k_{2_o} are proportional to v and v^2 , respectively. The tail-tip amplitude y_{\max} , however, remains constant, keeping the Strouhal number also constant. The results from the optimal gait closely match the data of live saithe when the precaudal stiffness is approximately 85% of the caudal stiffness. Snapshots of the optimal body motion are shown in figure 7 for $k_1 = 0.85k_{2_o}$, where the fish is swimming with an oscillation frequency of 3.52 Hz. The swimming motion in figure 7 closely resembles the observed swimming in figure 4. Thus, saithe appears to minimize active muscle bending moment during steady-state swimming by adjusting its gait, tail-beat frequency, and body stiffness.

3.2.2 Optimal Gait Exploits Resonance

[Figure 7 about here.]

We will present an analytical explanation for the optimal frequency ω_o and why it is proportional to swimming speed. We theorize that both body resonance and fluid resonance are exploited in natural swimming. As in Section 3.1.1, we use the fact that our model saithe features $A_1 \cong A_2 := A_o$ to understand how optimal, and hence natural, gait exploits resonance.

When a sinusoidal bending moment of frequency ω is applied to the anterior tail joint, the tail tip oscillates laterally at the same frequency. For a unit amplitude of the bending moment, the maximum tail-tip velocity depends on the driving frequency, and is given by the absolute value of the so-called frequency response, denoted by $|Q(j\omega)|$. According to the optimal gait theory, the minimum amplitude of bending moment that achieves average speed v is given by

$$\max_t |u_1(t)| = \frac{\pi v \cdot St}{|Q(j\omega)|}.$$

Thus, the optimal frequency that minimizes the active muscle tension cost is the resonance frequency that maximizes the tail-tip velocity for a given magnitude of the bending moment. Since swimming speed is proportional to maximum tail-tip speed, (1), we can also interpret the resonance with the frequency that maximizes the ratio of swimming speed to input torque magnitude.

To verify existence of resonance, we consider the optimal locomotion example shown in figure 7, where the optimal frequency is $\omega_o = 3.52$ Hz. The plot of the amplification factor $|Q(j\omega)|$ as

a function of frequency ω is shown in figure 9. There is a well-defined resonance peak that maximizes $|Q(j\omega)|$ at 3.51 Hz. Because of the slight difference between A_1 and A_2 , there is a negligible difference between the optimal frequency ω_o and the resonance frequency.

3.2.3 Hydrodynamics and Body Flexibility Resonate

The previous two sections have shown that a swimming saithe exploits resonance to achieve a desired speed with minimal muscle load. This section explores the origin of the resonance. When the fish body is flexible, there may exist a peak resonance of the transfer function $Q(j\omega)$, that is close to the fish body's natural frequency. But it is possible that this resonance is also related to a hydrodynamic resonance due solely to the fluid. We separately examine these two possible sources of resonance.

Without fluid, resonance exists within the fish body itself, resulting from the body's inertia and stiffness. For the swimming fish shown in figure 7, the first two resonance frequencies of the body are 1.12 and 6.13 Hz, which are in the same order as the resonance frequency $\omega_r = 3.52$ Hz for the coupled body-fluid system at velocity 1.2 m/s, but are not very close. Alternatively, the resonance frequencies can be defined using the effective inertia containing both body and added-mass. This corresponds to the resonance frequencies of the body in still water, which are at 0.49 Hz, and 3.29 Hz. Therefore, the tail-beat frequency of optimal (and natural) swimming is close to the second natural mode of oscillation resulting from body flexibility and total effective mass.

To study hydrodynamic resonance, we remove the fish body's mass and stiffness, and assume that the fish model can achieve an arbitrary tail motion through bending moment inputs at both joints. In this case, the transfer function from bending moments to lateral tail-tip velocity, denoted by $Q_F(s)$, contains the fluid inertia and skewed damping due to fluid flow. Although the body lacks stiffness, there is still a well-defined peak that maximizes the gain of $Q_F(s)$ as shown in figure 10. This resonance occurs at $\omega_r = 2.4$ Hz, which is reasonably close to the natural swimming frequency at 3.5 Hz. Figure 8 depicts snapshots of the optimal gait when there is no body mass or stiffness. Because the optimal frequency is 2.4 Hz, and the swimming speed is 1.2 m/s, the tail-tip amplitude is larger than in observed swimming, so the Strouhal number remains at 0.2.

4 Discussion

The results in this paper are derived from a simple fish swimming model, with hydrodynamic forces modeled as static functions of relative velocity and acceleration. Due to the approximations, our results may not be exactly accurate in a quantitative sense, and we remain cautious when interpreting the results. Nevertheless, the model presumably captures essential dynamics of fish swimming, and the results should provide basic understanding of swimming mechanisms. The results are applicable when the body can be roughly separated into a main body and tail sections, the main body's lateral motion is negligible compared to the tail motion, and reactive force model for thrust generation is valid.

4.1 Power Equality for Lateral Kinetic Loss and Thrust

The total power used in swimming is found to be invariant over various gaits; it is always equal to $2cv^3$, twice the power loss due to resistive drag, regardless of the hydrodynamic parameter values, and is proportional to the swimming speed cubed. Therefore, power optimality cannot be the reason why fish consistently choose particular gaits. Note, however, that the "total power" we examined is the mechanical power output from muscle that is eventually dissipated into water; power loss

associated with muscle activation is not considered. If the activation cost is considered, it may perhaps explain the natural gait by power optimality.

Fish swim by transferring a supply of power between their muscles, their tail, and the water. Figure 11 shows a diagram of this energy transfer. First, muscles provide a total average supply of power, \bar{E} , to the tail, through bending moment input. The tail transfers this energy to the water as the rate of work \bar{Y} done in the lateral direction; $\bar{E} = \bar{Y}$. The water then gains a portion as kinetic power, \bar{T} , and returns the rest, $\bar{P}v$, to the tail for thrust generation; $\bar{Y} = \bar{T} + \bar{P}v$. The thrust power is eventually dissipated as heat, \bar{D} , through resistive drag on the body; $\bar{P}v = \bar{D}$. Overall, the total power supplied by muscle is lost into water in two forms, $\bar{E} = \bar{D} + \bar{T}$. The loss due to drag, $\bar{D} = cv^3$, is a price to be paid regardless. The additional loss, \bar{T} , is the overhead cost required when generating thrust by pushing water in the lateral direction. A major finding of our analysis is that, to generate thrust power $\bar{P}v$, fish has to waste the same amount of power in the lateral direction as the rate of kinetic energy gained by water; $\bar{T} = \bar{P}v$.

[Figure 8 about here.]

Because of the equality between kinetic power \bar{T} and thrust power $\bar{P}v$, our result predicts that the ratio of useful power to total power, known as Froude efficiency, $\eta := \bar{P}v/\bar{E}$, is exactly $1/2$, regardless of the gait, swim speed, or driving frequency. Biological data [14] indicate that η is in the range 0.52 – 0.72 for steadily swimming saithe, which is larger than the predicted value $1/2$. We suspected that a large portion of the error is attributed to the model approximation, and studied the power transfer of the original nonlinear model from which the simpler model was derived. The original nonlinear model contains trigonometric terms of θ , including the nonlinear acceleration term for reactive hydrodynamic forces as in [25]. As expected, simulations of the nonlinear model give more realistic values of Froude efficiency that are larger than or less than $1/2$, depending on the gait, frequency, and speed. Thus, we predict $\eta \approx 1/2$ for swimming with small oscillation amplitude. Higher Froude efficiency ($\eta > 0.8$) of thunniform swimming [33] cannot be predicted by our model since the main thrust source is lift force rather than added-mass effect [34].

4.2 Invariance of Strouhal Number

The Strouhal number St describes the wake structure in fish swimming. Fish and cetaceans generally swim with St between 0.2 – 0.4 , with the saithe St lying on the lower end of this interval [27]. Biological data of a variety of fish, including dace, trout, goldfish, and jack mackerel, have pointed to a linear relationship between oscillation frequency and swim speed, and a direct relationship between tail-tip amplitude and body length. Based on these results, various literature have concluded that St remains constant for a fixed ratio of swim speed to tail-beat frequency v/ω [5, 35]. According to our analysis, thrust-drag balance requires the ratio of swim speed to maximum tail-tip speed v/v_t , and therefore St , be a constant depending on only the fish's body geometry and hydrodynamic parameters. The optimality for small tension then explains the observed proportionality of frequency and constancy of tail-tip amplitude with respect to speed.

Interestingly, [36] observed that St is a function of a single parameter called the Lighthill number $Li := c_D A_w / b^2$, where b is the tail tip height. If the volume of fluid accelerated by tail is estimated by a circular cylinder of diameter αb with a constant α depending on the tail geometry, then the cross-sectional area of the added mass is $A_o = \pi(\alpha b/2)^2$, and the formula in (2) reduces to $St = (2/\pi)^{3/2} \sqrt{Li}/\alpha$, explicitly showing the dependence of St on Li . Moreover, this simple formula with $\alpha \approx 0.5$ explains the (Li, St) relationships for many species in Fig. 4 of [36]. While [36] interpreted the result through power optimality, our analysis derives this formula from thrust-drag balance without optimality.

Experimental data from oscillating foil in fluids have demonstrated maximum Froude efficiency η for St in the range of 0.25-0.35 due to efficient thrust development [8, 12, 37]. There is an apparent discrepancy between these results and our results, which state that St is independent of gait optimality. This discrepancy arises because the literature defines wake resonance as maximum spatial amplification of unstable flow, while our St results follow from the assumption of thrust-drag balance. In the oscillating airfoil experiments, the flow speed is fixed independently of the imposed amplitude and frequency, and hence thrust and drag may not balance. Our results predict that if the flow speed is adjusted to achieve thrust-drag balance, the St will remain fairly constant.

4.3 Optimality of Natural Swimming

To determine whether the periodic body motion in natural swimming is optimal, we found the gait that minimizes muscle bending moment, and compared the results to data of live saithe swimming. The model was adjusted to have an active anterior tail and a passive caudal tail fin, to capture the anatomy of live fish. Because no data is available on the body stiffness of swimming saithe, we included the stiffness as an optimization parameter, with a fixed ratio of precaudal stiffness k_1 to caudal stiffness k_2 . Our choice to adjust stiffness while keeping k_1/k_2 constant was based on the observation that local body flexibility is related to the muscle activation level and body curvature at the site.

The total bending stiffness is determined by the active and passive stiffness of the muscle-tendon-skin system and the vertebral column stiffness [38, 3]. Experimental results on stiffness properties of blue marlin [39] and longnose gar [4] suggest that caudal intervertebral joints have a higher stiffness than precaudal joints, and increasing bending amplitude increases body stiffness. In swimming fish, the ratio of bending amplitudes at 50% to 70% of the body length is approximately 0.80 and 0.55 for curvature and strain of mackerel [40] and 0.63 for curvature of saithe [13]. These studies indicate that the stiffness in the caudal region should be greater than the precaudal region due to higher curvature/strain. Consistent with these results, comparison of model-predicted optimal gaits with observed gaits of live saithe suggested that the precaudal stiffness k_1 is about 85% of the caudal stiffness k_2 .

The results demonstrated that characteristics of natural gaits over a range of swimming speeds can be explained by optimality of minimum bending moment. In particular, the data collected from live saithe swimming indicated that the oscillation frequency linearly increases with speed while tail-tip amplitude remains constant. These properties are captured by the optimal gaits with frequency and amplitude values close to observations (figure 6). The linearly increasing frequency can be explained in terms of optimality, together with resonance mechanisms. The constancy of the amplitude then follows from the constancy of the Strouhal number. Because these numerical results match tendencies observed in live fish swimming, and the optimal body shape is close to the observed gait, we stipulate that the optimal gait which minimizes muscle tension can explain carangiform locomotion.

4.4 Resonance Mechanisms Underlying Swimming

An essential question in animal locomotion is how animals choose a specific oscillation frequency to achieve a desired velocity. Most biological observations hint at the exploitation of natural dynamics associated with the interaction of the (flexible) body and environment in order to reduce energy consumption [41]. Additionally, experimental data from oscillating foils have demonstrated the existence of a “wake resonance,” which maximizes thrust production [8]. Numerical and experimental studies of flexible foils oscillating in fluids have found resonance peaks to be a function of imposed flow and wing rigidity [42, 43]. Based on these results, we predicted that natural fish

swimming is exploiting some type of resonance, due to a combination of natural body frequency and hydrodynamic resonance. Our results confirmed this prediction. We found that natural gait is optimal with respect to minimum bending moment, and the optimal gait exploits resonance to maximize the tail-tip velocity. Therefore, we conclude that there are resonance mechanisms underlying natural swimming gaits.

The results demonstrated that fish swims faster by increasing its oscillation frequency. Because the tail oscillation exploits resonance, the body adjusts its stiffness so that the resonance frequency matches the frequency required to achieve a desired speed. This result agrees with the frequency tuning theory observed in animals [4, 7, 41]. The model analytically predicts that optimal tail-beat frequency ω and tail stiffness K are proportional to v and v^2 , respectively, and the optimal tail-beat amplitude stays constant over a range of swimming speeds. Many fish exhibit the proportionality and constancy properties [8], hence our result may suggest resonance exploitation in general fish swimming.

A remaining question is: what is the origin of the resonance? Consider a virtual experiment where the fish body is fixed in a flow tank to experience fluid flow at velocity v . If a sinusoidal bending moment of fixed amplitude is applied to flip the tail, there is a frequency where the amplitude of the lateral tail velocity is maximum; this is the resonance observed in figure 9. In Section 3.2.3, we found that this resonance is still observed when we remove the body mass and stiffness. Thus, the origin of the overall resonance may be traced to the dynamics without body. Because this peak is purely due to fluid effects, we call it a hydrodynamic resonance. However, its relation to the so-called wake resonance [12] is not obvious since the latter is unrelated to muscle bending moment.

The hydrodynamic resonance found in Section 3.2.3 may be explained by the natural oscillation resulting under no muscle moment input, thereby making a possible connection to the wake resonance. With no input or body inertia/stiffness, the tail motion is governed by natural dynamics with complex eigenvalues; therefore an ideal fish body with no mass/stiffness can naturally oscillate in a flow without muscle input. The natural oscillation could be exploited to resonate the tail motion with the input excitation. The period of the natural oscillation can be analytically derived for the simplified case, where the precaudal and caudal panels are assumed equal ($l_1 = l_2$, $A_1 = A_2$), as follows:

$$\tau_{\text{nat}} = \left(\frac{14\pi}{12\sqrt{3}} \right) \left(\frac{l_t}{v} \right) \cong 2 \left(\frac{l_t}{v} \right), \quad (4)$$

where l_t is the total tail length. As expected, the natural frequency $\omega_{\text{nat}} := 2\pi/\tau_{\text{nat}}$ is close to the resonance frequency; for instance, $\omega_{\text{nat}} = 2.84$ Hz for $v = 1.2$ m/s and $l_t = 0.2$ m. The analytical formula (4) shows that the natural oscillation is presumably related to how water travels across the tail. The tail flips from left to right in roughly l_t/v seconds, equal to the time it takes for water to flow through the length of the tail. Thus, the caudal tail may take advantage of the water accelerated by the precaudal section.

We have found that both hydrodynamic resonance and body resonance exist separately, and they are reasonably close to the overall resonance and hence to the cycle frequency of natural swimming. While body resonance frequency can be adjusted by active muscle stiffness, hydrodynamic resonance frequency is determined essentially by the ratio of the swimming speed to the total tail length. Therefore, our results suggest the following mechanisms underlying natural swimming: body geometry determines the hydrodynamic resonance to be exploited for swimming at a desired speed, muscle stiffness is actively adjusted in proportion to the speed squared so that body resonance is roughly aligned with the hydrodynamic resonance, then the muscle bending moment drives the tail to excite the overall body-fluid resonance.

Acknowledgments: This work is supported by NSF No.1335545 and ONR N00014-08-1-0642.

References

- [1] Long, J. H. & Nipper, K. S. 1996 The importance of body stiffness in undulatory propulsion *Amer. Zool.* **36**, 678-694. (DOI 10.1093/icb/36.6.678)
- [2] Long, J. H. 1998 Muscles, Elastic Energy, and the Dynamics of Body Stiffness in Swimming Eels *Amer. Zool.* **38**, 771-792. (DOI 10.1093/icb/38.4.771)
- [3] Pabst, D. A. 1996 Springs in swimming animals *Amer. Zool.* **36**, 723-735. (DOI 10.1093/icb/36.6.723)
- [4] Long, J. H., Hale, M. E., McHenry, M. J., & Westneat, M. W. 1996 Functions of fish skin: flexural stiffness and steady swimming of longnose gar *Lepisosteus Osseus J. Exp. Biol.* **199**, 2139-2151.
- [5] Bainbridge R. 1958 The speed of swimming of fish as related to size and to the frequency and amplitude of the tail beat *J. Exp. Biol.* **35**, 109-133.
- [6] Webb, W. P., 1973 Effects of partial caudal-fin amputation on the kinematics and metabolic rate of underyearling sockeye salmon (*Oncorhynchus nerka*) at steady swimming speeds, *J. Exp. Biol.* **59**, 565-581.
- [7] McHenry, M. J., Pell, C. A., & Long, J. H. 1995 Mechanical control of swimming speed: stiffness and axial wave form in undulating fish models *J. Exp. Biol.* **198**, 2293-2305.
- [8] Triantafyllou, G. S. 1993 Optimal thrust development in oscillating foils with application to fish propulsion *J. Fluid and Struc.* **7**, 205-224. (DOI 10.1006/jfls.1993.1012)
- [9] Taylor, G.K., Nudds, R.L., Thomas, A.L.R. 2003 Flying and swimming animals cruise at a Strouhal number tuned for high power efficiency *Nature* **425**, 707-711.
- [10] Triantafyllou, M. S., Triantafyllou, G. S., & Yue D. K. P. 2000 Hydrodynamics of fishlike swimming *Annu. Rev. Fluid Mech.* **1**, 33-53. (DOI 10.1146/annurev.fluid.32.1.33)
- [11] Lewin, G.C., Haj-Hariri, H. 2003 Modelling thrust generation of a two-dimensional having airfoil in a viscous flow *J. Fluid Mech.* **492**, 339-362.
- [12] Moored, K. W., Dewey, P. A., & Smits, A. J. & Haj-Hariri, H. 2012 Hydrodynamic wake resonance as an underlying principle of efficient unsteady propulsion *J. Fluid Mech.* **708**, 329-348. (DOI 10.1017/jfm.2012.313)
- [13] Hess, F. & Videler, J.J. 1984 Fast continuous swimming of saithe (*Pollachius virens*): a dynamic analysis of bending moments and muscle power *J. Exp. Biol.* **109**, 229-251.
- [14] Videler, J. J. & Hess, F. 1984 Fast continuous swimming of two pelagic predators, saithe (*Pollachius virens*) and mackerel (*Scomber scombrus*): a kinematic analysis *J. Exp. Biol.* **109**, 209-228.
- [15] Cheng, J.Y., Pedley, T.J., & Altringham, J.D. 1997 A continuous dynamic beam model for swimming fish *Phil. Trans. R. Soc. Lond.* **353**, 981-997. (DOI 10.1098/rstb.1998.0262)
- [16] Lighthill, M. J. 1960 Note on the swimming of slender fish *J. Fluid Mech.* **9**, 305-317. (DOI 10.1017/S0022112060001110)
- [17] Lighthill, M. J. 1970 Aquatic animal propulsion of high hydrodynamic efficiency *J. Fluid Mech.* **44**, 265-301. (DOI 10.1146/annurev.fl.01.010169.002213)
- [18] Lighthill, M. J. 1971 Large-amplitude elongated-body theory of fish locomotion *Proc. R. Soc. Lond.* **179**, 125-138. (DOI 10.1098/rspb.1971.0085)
- [19] Blair, J. & Iwasaki, T. 2011 Optimal gaits for mechanical rectifier systems *IEEE Trans. Autom. Control* **56**, 59-71. (DOI 10.1109/TAC.2010.2051074)

- [20] Chen, J., Friesen, W. O., & Iwasaki, T. 2012 Mechanisms underlying rhythmic locomotion: interactions between activation, tension and body curvature waves *J. Exp. Biol.* **215**, 211-219. (DOI 10.1242/jeb.058669)
- [21] Blight, A. R. 1977 The muscular control of vertebrate swimming movements *Biol. Rev.* **52**, 181-281. (DOI 10.1111/j.1469-185X.1977.tb01349.x)
- [22] Long, J. H., McHenry, M. J., & Boetticher, N. 1994 Undulatory swimming: how traveling waves are produced and modulated in sunfish *J. Exp. Biol.* **192**, 129-145.
- [23] Altringham, J. D., Wardle, C. S., & Smith, C. I. 1993 Myotomal muscle function at different locations in the body of a swimming fish *J. Exp. Biol.* **182**, 191-206.
- [24] Daniel, T. L. 1984 Unsteady aspects of aquatic locomotion *Amer. Zool.* **24**, 121-134. (DOI 10.1093/icb/24.1.121)
- [25] Chen, J., Friesen, W. O., & Iwasaki, T. 2011 Mechanisms underlying rhythmic locomotion: body-fluid interaction in undulatory swimming *J. Exp. Biol.* **214**, 561-574.
- [26] Saito, M., Fukaya, M., & Iwasaki, T. 2002 Serpentine locomotion with robotic snakes *IEEE Contr. Sys. Magazine* **22**, 64-81.
- [27] Rohr, J. J. & Fish, F. E. 2004 Strouhal numbers and optimization of swimming by Odontocete cetaceans *J. Exp. Biol.* **207**, 1633-1642. (DOI 10.1242/jeb.00948)
- [28] Sundnes, G. 1963 Studies on the high nitrogen content in the physostome swimbladder *Rept. Norweg. Fishery Invest.* **13**, 1-8.
- [29] Magnuson, J. J. 1978 Locomotion by scombrid fishes: Hydrodynamics, morphology, and behavior *Fish Physiology* **7**, 240-315.
- [30] Fierstine, H. L., & Walters, V. 1968 The propulsion of the sea-urchin spermatozoa *J. Exp. Biol.* **32**, 802-814.
- [31] Ahlborn, B., Harper, D. G., Blake, R. W., Ahlborn, D., & Cam, M., 1991 Fish without footprints *J. Theor. Biol.* **148**, 521-533. (DOI 10.1016/S0022-5193(05)80234-6)
- [32] Tytell, E. D. 2004 Kinematics and hydrodynamics of linear acceleration in eels, *Anguilla rostrata* *R. Soc. Lond.* **271**, 2535-2540. (DOI 10.1098/rspb.2004.2901)
- [33] Fish, F. E., Rohr, J. J. 1999 Review of dolphin hydrodynamics and swimming performance, *SPAWARS System Center Technical Report 1801*. San Diego, CA.
- [34] Sfakiotakis, M., Lane, D. M., Bruce, J., Davies, B. C. 1999 Review of fish swimming modes for aquatic locomotion, *IEEE J. Ocea. Eng.* **24**, 237-252. (DOI 10.1109/48.757275)
- [35] Hunter, J. R. & Zweifel, J. R. 1971 Swimming speed, tail beat frequency, tail beat amplitude, and size in jack mackerel *Trachurus symmetricus* and other fishes *Fishery Bulletin* **69**, 253-266.
- [36] Eloy, C. 2012 Optimal Strouhal number for swimming animals *J. Fluid Mech.* **30**, 205-218. (DOI 10.1016/j.jfluidstructs.2012.02.008)
- [37] Ohashi, H. & Ishikawa, N. 1972 Visualization study of a flow near the trailing edge of an oscillating foil *Bulletin of the Japanese Soc. of Mech. Eng.* **15**, 840-845. (DOI 10.1299/jsme1958.15.840)
- [38] Brainerd, E. L. & Patek, S. N. 1998 Vertebral column morphology, C-start curvature, and the evolution of mechanical defenses in tetraodontiform fishes *Copeia* **1998**, 971-984.
- [39] Long, J. H. 1992 Stiffness and damping forces in the intervertebral joints of blue marlin (*Makaira nigricans*) *J. Exp. Biol.* **162**, 131-155.

- [40] Shadwick, R. E., Steffensen, J. F., Katz, S. L., & Knower, T. 1998 Muscle dynamics in fish during steady swimming *Amer. Zool.* **38**, 755-770. (DOI 10.1093/icb/38.4.755)
- [41] Ahlborn, B. K., Blake, R. W., & Megill W. M. 2006 Frequency tuning in animal locomotion *Zoology* **109**, 43-53. (DOI 10.1016/j.zool.2005.11.001)
- [42] Michelin, S., Llewellyn Smith, S. G. 2009 Resonance and propulsion performance of a heaving flexible wing *Physics of Fluids* **21**, 071902. (DOI 10.1063/1.3177356)
- [43] Alben, S., Witt, C., Vernon Baker, T., Anderson, E., Lauder, G.V. 2012 Dynamics of freely swimming flexible foils *Physics of Fluids* **24**, 051901. (DOI 10.1063/1.4709477)

Appendix

[Table 2 about here.]

The saithe fish is modeled with a main body and two undulating panels with two rotating joints, as described in Section 2.1. The variables are summarized in Table 3. The resistive drag force f_o and reactive forces and torques f_i and τ_i acting on the body are modeled as

$$f_o = -\text{sgn}(\dot{x}_o)c\dot{x}_o^2, \quad f_i = m_{A_i}a_i/\cos\theta_i, \quad \tau_i = -(m_{A_i}l_i^2/3)\ddot{\theta}_i,$$

for $i = 1, 2$, where

$$c := \frac{1}{2}c_D\rho A_w, \quad m_{A_i} := \rho V_i c_{A_i} = \rho(2l_i)A_i, \quad V_i := \pi(d_i/2)^2(2l_i), \quad A_i := \pi(d_i/2)^2 c_{A_i}.$$

The kinematic and dynamic equations are given by:

$$\begin{aligned} x_1 &= x_o + l_o + l_1 \cos\theta_1, & m_o \ddot{x}_o &= g_{x_1} + f_o + \xi, \\ x_2 &= x_1 + l_1 \cos\theta_1 + l_2 \cos\theta_2, & m_1 \ddot{x}_1 &= f_1 \sin\theta_1 - g_{x_1} + g_{x_2}, \\ y_1 &= y_o + l_1 \sin\theta_1, & m_2 \ddot{x}_2 &= f_2 \sin\theta_2 - g_{x_2}, \\ y_2 &= y_1 + l_1 \sin\theta_1 + l_2 \sin\theta_2, & m_1 \ddot{y}_1 &= -f_1 \cos\theta_1 - g_{y_1} + g_{y_2}, \\ w_i &= \dot{y}_i - \dot{x}_i \theta_i, & m_2 \ddot{y}_2 &= -f_2 \cos\theta_2 - g_{y_2}, \\ a_i &= \ddot{y}_i - \ddot{x}_i \theta_i - 2\dot{x}_i \dot{\theta}_i, & J_1 \ddot{\theta}_1 &= \tilde{u}_2 - \tilde{u}_1 + \tau_1 - (g_{x_1} + g_{x_2})l_1 \sin\theta_1 + (g_{y_1} + g_{y_2})l_1 \cos\theta_1, \\ & & J_2 \ddot{\theta}_2 &= -\tilde{u}_2 + \tau_2 - g_{x_2}l_2 \sin\theta_2 + g_{y_2}l_2 \cos\theta_2, \end{aligned}$$

where ξ is an external force acting on the main body, $J_i := m_i l_i^2/3$ is the i th panel's moment of inertia, g_{x_i} and g_{y_i} are constraint forces due to the neighboring panel(s), and \tilde{u}_i are the total bending moments containing the effects of active muscle and body flexibility:

$$\tilde{u}_1 = u_1 + k_1 \theta_1, \quad \tilde{u}_2 = u_2 + k_2 (\theta_2 - \theta_1).$$

The dynamic equations involving $m_i \ddot{x}_i$ and $m_i \ddot{y}_i$ can be solved for the constraint forces g_{x_i} and g_{y_i} ; these expressions are substituted into the equations involving $m_o \ddot{x}_o$ and $J_i \ddot{\theta}_i$ to derive nonlinear equations of motion.

We consider the situation where ξ regulates the swim speed such that $\dot{x}_o(t) = -v$ with a constant $v > 0$. The average of the external force $\xi(t)$ over one cycle should be zero such that average thrust balances average drag:

$$\bar{\xi} = 0 = \overline{f_1 \sin\theta_1 + f_2 \sin\theta_2 + f_o},$$

where the notation \bar{z} for a τ -periodic signal z means the average $\bar{z} := (1/\tau) \int_0^\tau z(t) dt$. Assuming small $\theta_i = O(\epsilon)$ and neglecting $O(\epsilon^2)$ terms in the tail motion equation and $O(\epsilon^3)$ terms in the thrust drag balance equation, we find the following simplified equations of motion in vector form:

$$\begin{aligned} J\ddot{\theta} + 2vG\dot{\theta} + K\theta &= Bu, \\ \theta^\top G^\top \ddot{\theta} + cv^2 &= 0, \end{aligned} \quad (5)$$

where J, G, K , and B are constant 2×2 matrices representing the moment of inertia of the total effective mass, coefficient for reactive hydrodynamic torque, body stiffness, and transformation from bending moment to inertial torque, respectively. The matrices are defined by:

$$\begin{aligned} J &:= L(M + M_A)L/3 + F^\top(M + M_A)F, & G &:= F^\top M_A, & K &:= BK_oB, \\ F &:= \begin{bmatrix} l_1 & 0 \\ 2l_1 & l_2 \end{bmatrix}, & B &:= \begin{bmatrix} -1 & 1 \\ 0 & -1 \end{bmatrix}, & M &:= \text{diag}(m_1, m_2), & K_o &:= \text{diag}(k_1, k_2), \\ & & & & M_A &:= \text{diag}(m_{A_1}, m_{A_2}), & L &:= \text{diag}(l_1, l_2), \end{aligned}$$

where $\theta, u \in \mathbb{R}^2$ are stacked vectors of θ_i and u_i for $i = 1, 2$, respectively. This two-input case with $u \in \mathbb{R}^2$ is considered in Section 3.2.3. In all other analyses, the tail is assumed passive ($u_2(t) \equiv 0$), and u and B are redefined as $u := u_1$ and $B := [-1 \ 0]^\top$.

The optimal gait problem is formulated as follows. We apply sinusoidal bending moment $u_i(t) = a_i \sin(\omega t + b_i)$, where $a_2 = 0$ if the posterior joint is passive. Through the first equation in (5), the tail motion θ is determined as a function of frequency ω , amplitudes a_i , and phases b_i . Many choices of (ω, a_i, b_i) yield θ satisfying thrust-drag balance, or the second equation in (5). Among those, we choose (ω, a_i, b_i) that gives the smallest value of $a_1^2 + a_2^2$. The tail motion θ resulting from this input is the optimal gait. The theory [19] indicates that the optimal frequency is given by ω that maximizes the largest eigenvalue of matrix Z , and the optimal amplitudes/phases are specified by the corresponding eigenvector, where

$$Z := P_\omega^*(G + G^\top)P_\omega(\omega/v)^2/(2c), \quad P(s) := (Js^2 + 2vGs + K)^{-1}B,$$

and $P_\omega := P(j\omega)$ is the frequency response of the transfer function from bending moment u to tail angle θ . In Section 3.2, the transfer function $Q(s)$ is defined by $Q(s) := sl^\top P(s)$, and $Q_F(s)$ is obtained by setting $M = K = 0$ in $Q(s)$, where $l \in \mathbb{R}^2$ is a stacked vector of panel lengths.

Power equations (3) are obtained by multiplying (5) by $\dot{\theta}^\top$ and v , where

$$E := \dot{\theta}^\top Bu, \quad R := \dot{\theta}^\top J\ddot{\theta}, \quad V := \dot{\theta}^\top K\theta, \quad W := 2v\dot{\theta}^\top G\dot{\theta}, \quad \bar{D} := cv^3, \quad \bar{P} := -\overline{\theta^\top G^\top \ddot{\theta}}.$$

The rate of work done by the tail to water is $X = -v\theta^\top f$ and $Y = \dot{y}^\top f$ in the x and y -directions, respectively. $f \in \mathbb{R}^2$ is the force vector with entries f_1 and f_2 , and $y \in \mathbb{R}^2$ is the lateral displacement vector similarly defined. Following from the definitions, $\bar{W} = \bar{Y}$ and all muscle power $\bar{E} = \bar{W}$ is lost as the rate of work \bar{Y} done by the tail to water. Part of this power is returned from water to tail in the x -direction as the thrust power; $Pv = -X$. Hence, the difference $T := Y - Pv$ is the translational kinetic power gained by the fluid from the oscillating tail; $T = w^\top f$ where w is the lateral fluid velocity.

List of Figures

1	Top view of fish model. A large main body is constrained to move along the x -axis, and two oscillating panels represent the flexible tail section.	18
2	Hydrodynamic forces acting on the body model. Two snapshots at different time instants are shown with a lateral offset for clarity. The main body experiences resistive drag force f_o . The tail receives reactive hydrodynamic forces, f_1 and f_2 , due to the mass of fluid pushed in the lateral direction of the oscillating body. In steady swimming, the average reactive forces in the x -direction (thrust) balance the resistive drag. Reactive forces in the y -direction would balance the lateral resistive drag on the main body (not shown) if it were not constrained to only move in the x -direction.	19
3	Approximated side view of saithe.	20
4	Snapshots of observed swimming gait over a half cycle [13], with period τ , during steady-state swimming.	20
5	Estimation of the added-mass coefficients (virtual mass divided by nominal cylindrical mass) of the two tail links (c_{A_1}, c_{A_2}). For values on the two lines, average thrust and drag forces balance in the two observed gaits provided by [13], resulting in steady swimming. In the analysis, $c_{A_1} = 1$ and the average value of c_{A_2} for the two gaits (marked by a square) are used.	21
6	Results for optimal gait that minimizes muscle bending moment for the saithe model with a passive tail over a range of velocities. The tail joint stiffness is also optimized while the ratio of anterior stiffness to posterior stiffness is fixed. The data points indicated by “+” are from [14]. As the speed increases, the frequency linearly increases while the amplitude remains roughly constant so that St stays almost constant as analytically predicted. The optimal gaits are reasonably close to the observed data.	22
7	Snapshots of the optimal gait that minimizes muscle bending moment at a locomotion velocity of 1.2 m/s. The precaudal and caudal tail stiffnesses are optimized assuming $k_1/k_2 = 0.85$. The optimal oscillation frequency is 3.52 Hz and the optimal stiffness is $k_{2_o} = 0.117$ Nm/rad.	23
8	Snapshots of the hydrodynamically optimal gait. The conditions are the same as those for Fig. 7, except the fish model has no body mass or body stiffness, and both joints receive bending moment inputs. The optimal oscillation frequency is 2.38 Hz.	23
9	The gain of $Q(j\omega)$ over a range of frequencies, where $Q(s)$ is the transfer function from the muscle bending moment u_1 to the tail-tip velocity. The speed is $v = 1.2$ m/s and the tail stiffness is specified as $k_1 = 0.85k_2$ and $k_2 = 0.117$ Nm/rad. There is a peak, or resonance frequency at $\omega_r = 3.51$ Hz.	24
10	The gain of $Q_F(j\omega)$ over a range of frequencies, where $Q_F(s)$ is the transfer function from the muscle bending moments (u_1, u_2) to the tail-tip velocity when the fish has no body mass or body flexibility. There is a peak, or resonance frequency at $\omega_r = 2.4$ Hz.	24

11 Diagram of the energy transfer that occurs between the fish muscles, the main body and tail, and water. E is the total power supplied by muscle, Y is the rate of work done by tail to water in the lateral direction, P_v is the thrust power returned by water to tail, and D is the power loss due to resistive drag. 25

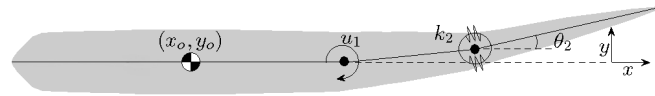


Figure 1: Top view of fish model. A large main body is constrained to move along the x -axis, and two oscillating panels represent the flexible tail section.

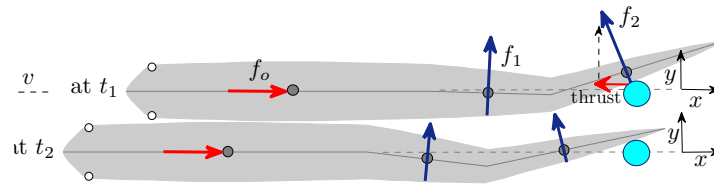


Figure 2: Hydrodynamic forces acting on the body model. Two snapshots at different time instants are shown with a lateral offset for clarity. The main body experiences resistive drag force f_o . The tail receives reactive hydrodynamic forces, f_1 and f_2 , due to the mass of fluid pushed in the lateral direction of the oscillating body. In steady swimming, the average reactive forces in the x -direction (thrust) balance the resistive drag. Reactive forces in the y -direction would balance the lateral resistive drag on the main body (not shown) if it were not constrained to only move in the x -direction.

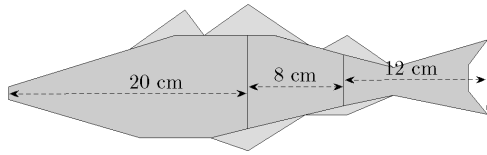


Figure 3: Approximated side view of saithe.

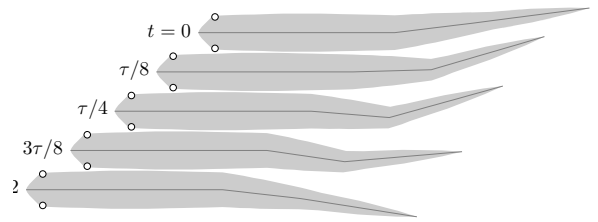


Figure 4: Snapshots of observed swimming gait over a half cycle [13], with period τ , during steady-state swimming.

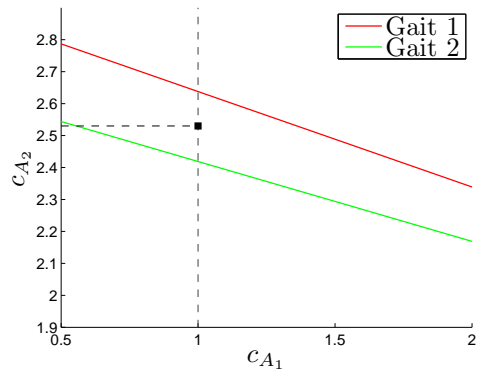


Figure 5: Estimation of the added-mass coefficients (virtual mass divided by nominal cylindrical mass) of the two tail links (c_{A_1}, c_{A_2}). For values on the two lines, average thrust and drag forces balance in the two observed gaits provided by [13], resulting in steady swimming. In the analysis, $c_{A_1} = 1$ and the average value of c_{A_2} for the two gaits (marked by a square) are used.

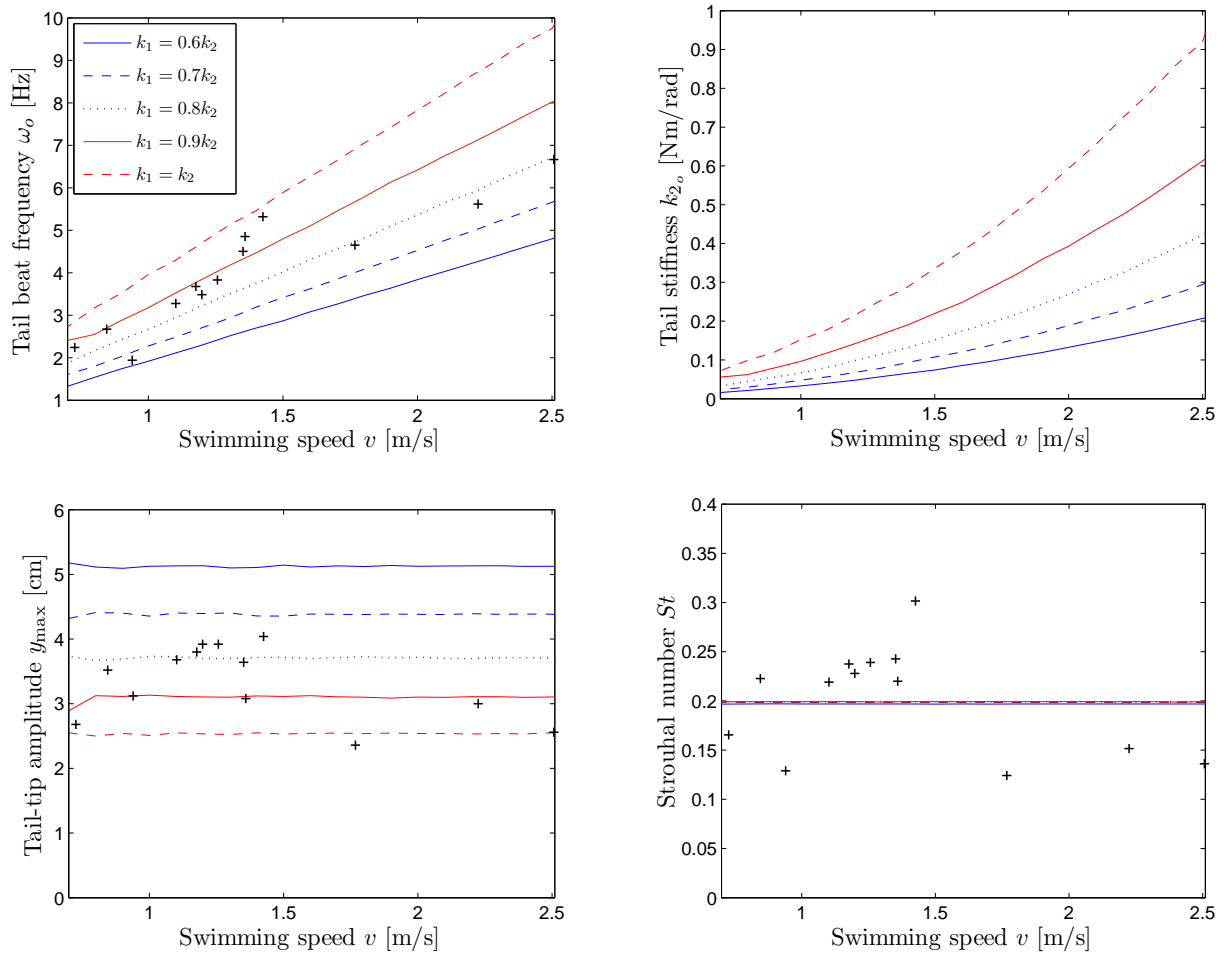


Figure 6: Results for optimal gait that minimizes muscle bending moment for the saithe model with a passive tail over a range of velocities. The tail joint stiffness is also optimized while the ratio of anterior stiffness to posterior stiffness is fixed. The data points indicated by “+” are from [14]. As the speed increases, the frequency linearly increases while the amplitude remains roughly constant so that St stays almost constant as analytically predicted. The optimal gaits are reasonably close to the observed data.

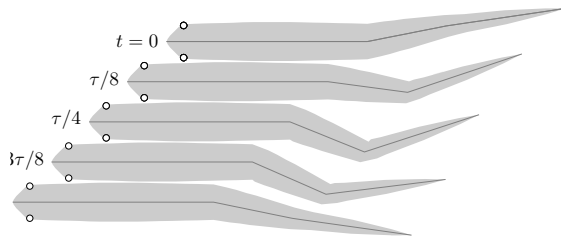


Figure 7: Snapshots of the optimal gait that minimizes muscle bending moment at a locomotion velocity of 1.2 m/s. The precaudal and caudal tail stiffnesses are optimized assuming $k_1/k_2 = 0.85$. The optimal oscillation frequency is 3.52 Hz and the optimal stiffness is $k_{2_o} = 0.117$ Nm/rad.

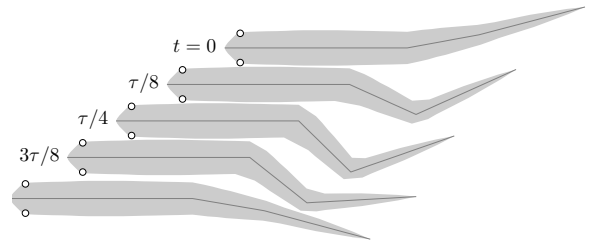


Figure 8: Snapshots of the hydrodynamically optimal gait. The conditions are the same as those for Fig. 7, except the fish model has no body mass or body stiffness, and both joints receive bending moment inputs. The optimal oscillation frequency is 2.38 Hz.

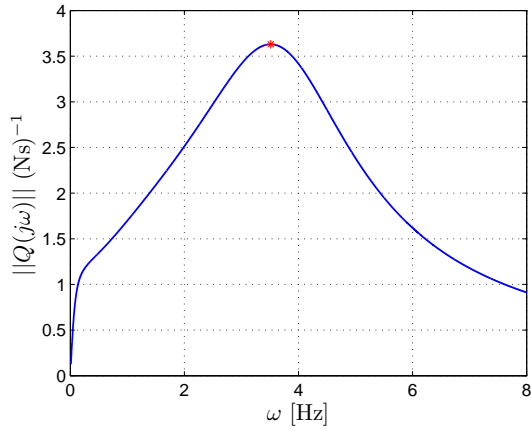


Figure 9: The gain of $Q(j\omega)$ over a range of frequencies, where $Q(s)$ is the transfer function from the muscle bending moment u_1 to the tail-tip velocity. The speed is $v = 1.2$ m/s and the tail stiffness is specified as $k_1 = 0.85k_2$ and $k_2 = 0.117$ Nm/rad. There is a peak, or resonance frequency at $\omega_r = 3.51$ Hz.

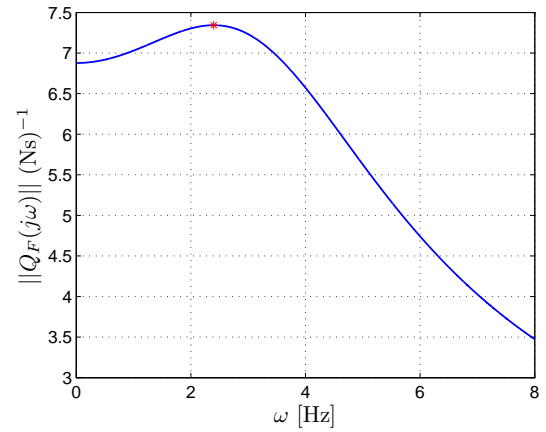


Figure 10: The gain of $Q_F(j\omega)$ over a range of frequencies, where $Q_F(s)$ is the transfer function from the muscle bending moments (u_1, u_2) to the tail-tip velocity when the fish has no body mass or body flexibility. There is a peak, or resonance frequency at $\omega_r = 2.4$ Hz.

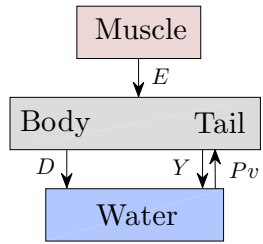


Figure 11: Diagram of the energy transfer that occurs between the fish muscles, the main body and tail, and water. E is the total power supplied by muscle, Y is the rate of work done by tail to water in the lateral direction, P_v is the thrust power returned by water to tail, and D is the power loss due to resistive drag.

List of Tables

1	Averaged body dimensions and kinematic data from saithe	27
2	Model parameters	27
3	List of model variables ($i = 1, 2$)	28

Table 1: Averaged body dimensions and kinematic data from saithe

total body length	$l_b = 0.40$ m
total body mass	$m = 11.3l_b^3$ kg/m ³
wetted surface area	$A_w = 0.401 l_b^2$
tail-beat period	$\tau = 0.278$ s
tail-beat amplitude	$h = 0.083 l_b$
swimming speed	$v = 0.86 l_b/\tau$

Table 2: Model parameters

	tail panel 1	tail panel 2
length	$2l_1 = 8$ cm	$2l_2 = 12$ cm
height	$d_1 = 6.09$ cm	$d_2 = 3.75$ cm
mass	$m_1 = 177$ g	$m_2 = 67.9$ g
fluid volume/length	$A_1 = 0.0182l_b^2$	$A_2 = 0.0174l_b^2$
added-mass coefficient	$c_{A_1} = 1$	$c_{A_2} = 2.53$
drag coefficient	$c_D = 0.009$	
water density	$\rho = 1000$ kg/m ³	

Table 3: List of model variables ($i = 1, 2$)

x_o	x -position of the center of mass (C.M.) of the main body
x_i	x -position of the C.M. of the i th panel
y_i	y -position of the C.M. of the i th panel
θ_i	angle between the i th panel and the x -axis
u_i	bending moment applied at joint i
w_i	velocity of fluid pushed by the i th panel in y direction
a_i	acceleration of fluid pushed by the i th panel